


Anticancer Activity and In Vitro to In Vivo Mechanistic Recapitulation of Novel Ruthenium-Based Metallodrugs in the Zebrafish Model

Brittany F. Karas ^{*,1} Jordan M. Hotz,^{*,†} Brian M. Gural,^{*} Kristin R. Terez,^{*} Victoria L. DiBona,^{*} Leonor Côrte-Real,[‡] Andreia Valente,[‡] Brian T. Buckley,[§] and Keith R. Cooper^{*}

^{*}Department of Biochemistry and Microbiology, Rutgers University, New Brunswick, New Jersey 08854, USA

[†]Laboratory of Cell Biology, Center for Cancer Research, National Cancer Institute, National Institutes of Health, Bethesda, Maryland 20892, USA

[‡]Centro de Química Estrutural and Departamento de Química e

Bioquímica, Faculdade de Ciências, Universidade de Lisboa, Lisboa 1749-016, Portugal and [§]Environmental and Occupational Health Sciences Institute, Rutgers University, Piscataway, New Jersey 08854, USA

¹To whom correspondence should be addressed at 89 French Street, New Brunswick, NJ 08901. E-mail: Brittany.karas@rutgers.edu.

ABSTRACT

Ruthenium is popular as a metal core for chemotherapeutics, due to versatile molecular coordination. Because new metallodrugs are synthesized at high rates, our studies included assays in zebrafish to expedite the initial evaluation as anticancer agents. Here we evaluated novel metallodrugs (PMC79 and LCR134), and cisplatin, a widely used platinum-based chemotherapeutic. We hypothesized that this model could characterize anticancer properties and recapitulate previous in vitro results in vivo. Our findings suggest anticancer properties of PMC79 and LCR134 were similar with less toxicity than cisplatin. Exposures from 24 to 72 h at or below the LOAELs of PMC79 and LCR134 (3.9 μ M and 13.5 μ M, respectively), impaired blood vessel development and tailfin regeneration. Blood vessel examination through live imaging of larvae revealed distinct regional antiangiogenic impacts. The significant decrease in gene expression of the VEGF-HIF pathway and beta-actin could explain the morphological effects observed in the whole organism following exposure. Tailfin amputation in larvae exposed to PMC79 or LCR134 inhibited tissue regrowth and cell division, but did not impact normal cell proliferation unlike cisplatin. This suggests Ru drugs may be more selective in targeting cancerous cells than cisplatin. Additionally, in vitro mechanisms were confirmed. PMC79 disrupted cytoskeleton formation in larvae and P-glycoprotein transporters in vivo was inhibited at low doses which could limit off-target effects of chemotherapeutics. Our results demonstrate the value for using the zebrafish in metallodrug research to evaluate mechanisms and off-target effects. In light of the findings reported in this article, future investigation of PMC79 and LCR134 are warranted in higher vertebrate models.

Key words: . metallodrugs; cisplatin; zebrafish; ruthenium; anticancer; P-gp pump; drug resistance; angiogenesis.

Platins or platinum-based metallodrugs are widely used in cancer treatment, however their efficacy is restricted by dose-limiting side effects and drug resistance (Hall et al., 2008;

Lieberthal et al., 1996; NCI 2014). Ruthenium (Ru) has become popular as a metal core due to its structural versatility (Abid et al., 2016; Alessio et al., 2004; Lin et al., 2018) and has shown a

Impact Statement

The objective of this research was to assess the specific modes of action for novel metallodrugs in a higher through-put model than rodents. The zebrafish model allows for mechanistic examination of whole organism effects, specific tissue effects, cellular and subcellular targets in an intact eukaryotic system. The culmination of this work has shown the zebrafish model as a powerful platform for the evaluation of novel Ru metallodrugs as well as their promising candidacy for evaluation in higher organisms.

potential to out-perform the platins in terms of decreased toxicity and targeted efficacy (Noffke et al., 2012). Two Ru-based drugs, NAMI-A and KP1019, had successfully entered clinical trials. NAMI-A, demonstrated antimetastatic properties in preclinical trials and did not recapitulate these results in patients. KP1019 showed anti-solid tumor effects and is currently being re-trialed using its sodium salt NKP1339/IT-139 (Alessio and Messori, 2019; Burris et al., 2016; Leijen et al., 2015; Lipponer et al., 1996; Trondl et al., 2014). Improvements in these metallodrugs involved manipulating the molecule to target characteristics of cancer, thereby improving delivery and limiting off-target effects.

Here we compare two Ru(II)-cyclopentadienyl (Cp)—(η^5 -C₅H₅) compounds as potential anticancer agents: PMC79, the Cp parental compound, and LCR134, a Cp derivative conjugated with biotin with the structures [Ru(η^5 -C₅H₅)(PPh₃)(2,2'-bipy-4,4-CH₂OH)]⁺ and [Ru(η^5 -C₅H₅)(PPh₃)(2,2'-bipy-4,4-dibiotin ester)]⁺, respectively (Figure 1) (Corte-Real et al., 2019; Côte-Real et al., 2019; Karas et al., 2019). These compounds belong to a novel class of Ru-based compounds which bear an organometallic fragment with proved cytotoxicity and improved aqueous stability (Moreira et al., 2019). Additionally, LCR134 contains two biotins (vitamin B7) in its structure for active targeting. Vitamin-drug targeting is a well-documented approach and is attributed to the upregulated expression of vitamin receptors on cancer cells from increased metabolic activity (Chen et al., 2010; Shi et al., 2014). Specifically, the biotin receptor, sodium-dependent multivitamin transporter, is overexpressed in various cancer cell lines (Ren et al., 2015; Tripodo et al., 2014).

The zebrafish model has become a powerful tool for screening large numbers of compounds and is in a unique position to provide a robust evaluation of in vitro endpoints. Zebrafish are an asset to pharmacology and toxicology as this model allows for examining adverse outcome pathways, in which cell culture lacks the complexity and rodent model are cost limiting. Large screening for drug activity and toxicity have been conducted in zebrafish and successfully identified compounds to be tested in clinical trials (Leonard and Randall, 2005; Santoriello and Zon, 2012; Tan and Zon, 2011). The aim of this study was to use an in vivo eukaryotic model to determine if alterations observed in vitro would be observed in the zebrafish model involving multiple cellular and organ systems. We hypothesized that anticancer activity initially discerned from in vitro studies would be confirmed in the context of a whole organism.

First, we established organism tolerability of PMC79 compared with our previous studies of LCR134 and cisplatin (Supplementary Tables 1 and 2) (Corte-Real et al., 2019; Karas et al., 2019). Using these data, we conducted gene expression analysis of key components of the VEGF-HIF pathway, which are highly conserved across vertebrates (Liang et al., 2001). Overexpression of these genes are correlated with poor patient prognosis, metastasis, and tumor resistance (Baba et al., 2010; Campbell et al., 2019; Chen et al., 2014; Zhan et al., 2017). In tandem, we conducted antiangiogenesis and regeneration studies

with markers of proliferation. Not only can we utilize the zebrafish model to assess direct toxicity at different levels of organization, the tailfin regenerating model can be used to examine wound repair processes that incorporate a number of genes that are relevant to tumor invasion and angiogenesis. Angiogenesis is pivotal in cancer progression as it provides a mechanism by which rapidly growing tissue can acquire nutrients, oxygen, and deplete toxic waste. In the developing zebrafish embryo angiogenesis and later in development vascular genesis/sprouting occurs, which allows for examination of both processes. Furthermore, angiogenesis is a hallmark of metastasis as blood vessel development provides an opportunity for cancerous cells to migrate (Zetter, 1998). Zebrafish can regenerate certain tissue including the fins. The caudal fin located at the posterior end of the body makes it easily accessible for surgical amputation. Larval fin regeneration offers an assay to assess impaired proliferation and remodeling of tissue. Fin regeneration allows for the examination of multiple factors and endpoints relevant to cell proliferation, migration, and differentiation. In our studies, LCR134 and PMC79 inhibited proliferation and regeneration with less toxicity than cisplatin. Additionally, our results showed that PMC79 exposure impaired site-specific angiogenesis.

According to previously published in vitro results, PMC79 accumulates in the membrane of cancer cells and causes disorganization of the cytoskeleton, specifically by depolymerization of F-actin (Moreira et al., 2019). Cytoskeleton inhibitors are a class of anticancer compounds which prevent cancerous cells from dividing. Early exposure of PMC79 to developing larvae confirmed cytoskeletal disorganization. Although LCR134 also accumulates in the cell membrane, its cellular interactions are distinct. PMC79 is transported by P-glycoprotein efflux transporter (P-gp pump), whereas LCR134 causes an inhibition of P-gp pump specific activity in NIH3T3 cells overexpressing this transporter (Corte-Real et al., 2019). This transporter is responsible for removing drugs from sites of action resulting in low efficacy and increased resistance. This resistance is correlated with poor prognosis and remains a limitation for chemotherapeutic treatment (Chung et al. 2016). As such, strategies to overcome P-gp-mediated resistance have become a target of drug development. The zebrafish studies were carried out to examine if similar effects could be reproduced in an in vivo model and a relevant vertebrate dose. Zebrafish express genes orthologous to ABCB1 called *abcb4* and *abcb5* that form a protein with similar structure, function, and pharmacological response (Cunha et al., 2017; Fischer et al., 2013; Zhu et al., 2019). These similarities have resulted in the successful use of the zebrafish model in evaluating P-gp protein activity. Specifically, the inhibition of this pump in zebrafish could have translational relevance result for overcoming chemotherapeutic resistance. We previously demonstrated that LCR134 can inhibit human P-gp in vitro (Corte-Real et al., 2019) and sought to investigate the clinical translatability of the zebrafish proteins. This endpoint has implications in chemotherapeutic treatment, as this transporter is one of the

most prominent causes of multidrug resistance (Pluchino *et al.*, 2012; Shaffer *et al.*, 2012). We investigated the ability of LCR134 to inhibit a homologous P-gp protein in zebrafish, Abcb1, both by cell culture flow cytometry and waterborne exposure in zebrafish larvae. Together, these studies provide evaluation of highly conserved and translatable biological processes that are critical targets of chemotherapeutic treatment.

MATERIALS AND METHODS

Zebrafish husbandry. The AB or the eGFP vascularly labeled transgenic Tg(fli1: EGFP)^{y1} strain zebrafish (Zebrafish International Resource Center, Eugene, Oregon) was used for all experiments. Breeding stocks less than 2 years postfertilization were bred and housed in Aquatic Habitats (Apopka, Florida) recirculating systems under a 14/10h light/dark cycle. System water was obtained by carbon/sand filtration of municipal tap water and water quality was maintained at <0.05 ppm nitrite, <0.2 ppm ammonia, pH between 7.2 and 7.7, and water temperature between 26°C and 28°C. All experiments were conducted in accordance with the zebrafish husbandry protocol and embryonic exposure protocol (no. 08-025) approved by the Rutgers University Institutional Animal Care and Use Committee. Males and females were maintained separately and co-mingled the night before breeding to allow spawning the next morning. Embryos were collected within 1 h after fertilization, removed of unfertilized embryos and stored in egg water (60 µg/ml Instant Ocean in DI water) until treatment.

Inductively coupled plasma-mass spectrometry (ICP-MS). Ru and cisplatin concentrations in solution and larval tissue were quantified by high-resolution ICP-MS (Nu Instruments Attom, Wrexham, UK). Data were recorded by the Attom software (Attolab v.1) as outlined previously (Karas *et al.*, 2019).

Metallo drug treatment and morphometric analysis. A modified fish embryo acute toxicity OECD protocol (OECD, 2013) was used in order to establish adverse outcomes and tissue development during PMC79 exposure. All treatments including the vehicle controls were maintained at or below 0.05% DMSO, a nontoxic dose previously established (Maes *et al.*, 2012). In the solvent control, no adverse effects were identified. Daily observations of individually housed embryos were recorded and included the following: death, lesions, yolk sac edema, and hemorrhaging. Zebrafish embryos were exposed to concentrations of PMC79 solutions (mg/l) at 0.05% of DMSO in individual glass vials through a waterborne exposure from 3 hours postfertilization (hpf) until 120 hpf (5 days) in a static nonrenewal protocol. Nominal zebrafish dose response concentrations 0, 3.1, 6.2, 9.2, 12.4 mg/l were determined using derivatives of an IC₅₀ value (3.1 mg/l) established following A2780 human ovarian cancer cells after 72 h (Corte-Real *et al.*, 2019). These doses were analytically determined to contain 0, 0.17, 0.44, 0.66, and 0.76 mg/l of Ru in previous work (Supplementary Tables 1 and 2) (Karas *et al.*, 2019). The exposure vials were continuously rocked on shaker platforms at 26°C for the duration of the study to insure constant egg exposure. PMC79 experiments were conducted as static nonrenewal. The dose response curve and morphometric analysis was conducted identically to previously published works for LCR134 and cisplatin in which two independent experiments from two different clutches were assessed (Corte-Real, 2019; Côte-Real, 2019; Karas, 2019, 2020). Each concentration included 20–30 larvae for a total of 40–60 independent biological replicates. The controls had >90% survival rate. Lesion

presence and death were recorded, during the major stages of organ development. A randomized portion of larvae surviving at the end of the toxicological experiment (120 hpf) were used for morphological data and included total body length as an indication of growth and development, pericardial sac size to evaluate cardiovascular impacts, yolk sac size for metabolic function and nutrient deposition and intraocular distance as an indication of craniofacial development (Supplementary Figure 1). Remaining larvae were quantified by ICP-MS Ru quantification analysis previously reported (Karas *et al.*, 2019).

Blood vessel measurements. Zebrafish blood vessel formation is very characteristic and has been thoroughly investigated. Development begins at around 12 hpf with all functioning vasculature developed by 72 hpf. A circulatory network containing the dorsal aorta (DA) and axial vein form around 24 hpf and blood circulates adjacent to the yolk sac through the Ducts of Cuvier (a large blood circulation sinus on the yolk sac where anterior and posterior cardinal vessels join) to begin sprouting of the subintestinal vessels (SIVs) into the gut (Fouquet *et al.*, 1997; Kimmel *et al.*, 1995; Serbedzija *et al.*, 1999).

Group-housed Tg(fli1: EGFP)^{y1} zebrafish embryos were treated with negative controls (egg water with 0.05% DMSO), a positive control of 23 mg/l sorafenib, a multikinase inhibitor that targets tumoral angiogenesis, and is used in the treatment of metastatic cancers, based on previously established literature (Chimote *et al.*, 2014), or doses of PMC79 or LCR134 at or below the lowest observed adverse effect level (LOAEL) established previously (Corte-Real *et al.*, 2019; Karas *et al.*, 2019). The treatments were conducted in 20 ml glass vials through a waterborne exposure beginning at 3 hpf in a static nonrenewal solution. Live animal imaging was conducted by anesthetizing larvae at 72 hpf in a 0.01% concentration of tricaine mesylate (MS-222) solution. This time point was selected in order to overlap with blood vessel development which begins at around 12 hpf with all functioning vasculature developed by 72 hpf. Larvae were then transferred onto 35 mm glass bottom dishes in 5% methyl cellulose and imaged using an Olympus TH4-100 inverted microscope with X-cite 120 Fluorescent Illumination. The subintestinal basket (SIV) area and branching number, and the intersegmental blood vessels (ISV) were measured using NIH ImageJ software. Three experimental replicates were conducted; N = 39–80.

In vivo reverse-transcriptase (RT) quantitative PCR. Group-housed zebrafish embryos were exposed to either egg water with 0.05% DMSO vehicle or doses of PMC79 or LCR134 at or below the LOAEL established previously (Corte-Real *et al.*, 2019; Karas *et al.*, 2019). All treatments contained at or below 0.05% of DMSO. The treatments were conducted in 20 ml glass vials through a waterborne exposure beginning at 3 hpf static nonrenewal solution. At 24 h, samples were rinsed 3×s with DI water and snap frozen in liquid nitrogen. This exposure time was chosen due to the high expression of the genes of interest during initial development. The genes investigated included vascular endothelial growth factors (*vegfa* and *c*), a mitogenic factor for angiogenesis; wingless-related integration (*wnt 3a* and *8a*), critical for upregulating *vegf*, cell growth, proliferation, and migration; as well as an inducer for all of these genes, hypoxia inducible factor α (*hif1 α*). Total RNA was isolated from 50 embryo composite samples using RNazol (Sigma-Aldrich). Reverse transcription was performed on 1 µg aliquots of RNA to produce cDNA for RT-PCR using a High-Capacity cDNA Reverse Transcription Kit (ThermoFischer) using a PTC-200 Peltier Thermal Cycler. RT-PCR

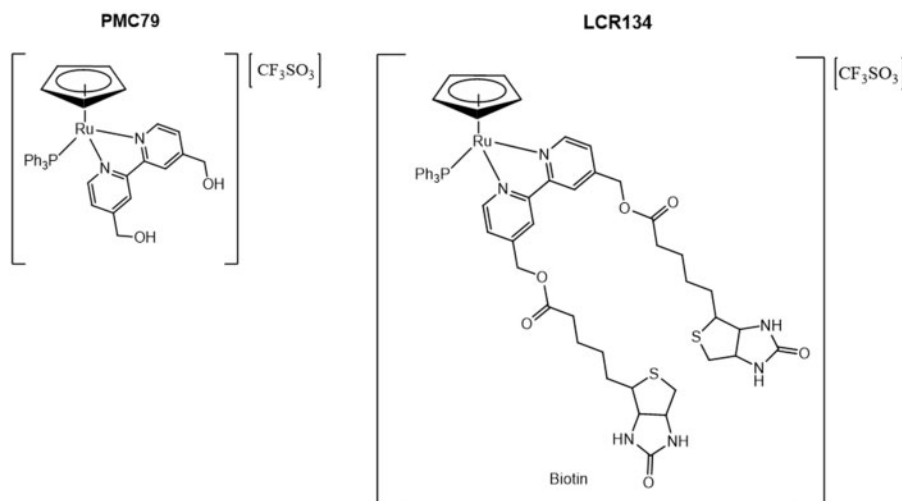


Figure 1. Chemical structures of PMC79 and LCR134. Two cyclopentadienyl ruthenium (Ru) metallodrugs: PMC79 (left) the parental compound, and LCR134 (right) containing 2 biotin conjugated to the bipyridine ligand.

reactions were performed in triplicate using PowerUp SYBR Green Master Mix (ThermoFischer) and the primers listed in [Supplementary Table 3](#). cDNA amplification was performed for 40 cycles on a QuantStudio 3 (Applied Biosystems) and recorded with QuantStudio Design and Analysis Software and analyzed in ThermoCloud (ThermoFischer). Analysis was conducted as $\Delta\Delta CT$ using 28S as an endogenous control. Three experimental replicates were conducted; $N = 9$.

Tail fin regeneration and PCNA/DAPI staining. Tg(fli1: EGFP)^{y1} strain zebrafish embryos were raised to 48 hpf and anesthetized in 0.01% MS-222. Tail fins were manually cut using a razor blade posterior to the notochord. Immediately following amputation, larvae were imaged and individually housed. Larvae were treated with either egg water with DMSO vehicle or doses of PMC79 or LCR134 at or below LOAEL, as established previously, for 24 h ([Corte-Real et al., 2019](#); [Karas et al., 2020](#)). This exposure time was selected based on the amount of time necessary for tissue regeneration and recovery. All treatments contained at or below 0.05% of DMSO and $5 \times 10^{-5}\%$ methylene blue to inhibit bacterial growth. At 24 hours postamputation (hpa), larvae were reimaged, sacrificed, and fixed in 4% paraformaldehyde (PFA) for 2–4 h at room temperature (RT). Fixed larvae were rinsed with PBS-T (rinse indicates 3 \times s for 5 min with phosphate-buffered saline + 0.1% Tween-20 [PBS-T]) and dehydrated in a methanol/PBST gradient (25%, 50%, 75%, 100%; 5 min each) and stored at -20°C until rehydration was conducted in the reverse gradient. After rehydration, larvae were PBST rinsed, and subsequently washed (1 \times ; 5min) and incubated in 150 mM Tris HCl, pH 9.0 incubate at 70°C for 15 min. Larvae were then permeabilized in prechilled acetone at -20°C for 10 min. Samples were then incubated in 10% normal horse serum (NHS)/PBST blocking buffer at 4°C for 3 h and subsequently anti-PCNA antibody [PC10] (ab29) (Abcam, Cambridge, UK) 1:500 NHS at rocked at 4°C for 3 days. Samples were then washed in 1% NHS block (5 \times s; 10 min) and incubated with DyLight 549 Horse Anti-Mouse IgG Antibody (Vector Labs) 1:1000 NHS at 4°C rocking for 2 days. After secondary incubation, samples were PBS-T rinsed and stored in Vectashield Antifade Mounting Medium with DAPI (Vector Laboratories, Burlingame, California) until fluorescent confocal imaging. Z-stack images were taken on an Olympus

FV1000MPE microscope (Olympus XLPlan N 25x objective NA 1.05) in $3\ \mu\text{m}$ step size. Z-stacks were compressed and ImageJ was used to count DAPI, PCNA and co-stained cells. Three experimental replicates were conducted and images were blinded; $N = 29\text{--}66$.

Cytoskeletal evaluation. Group-housed Tg(fli1: EGFP)^{y1} strain zebrafish embryos were collected and treated at 3 hpf with egg water with DMSO vehicle, $1\ \mu\text{g}/\text{ml}$ cytochalasin D (Millipore, St Louis, Missouri) or doses of PMC79 at or below LOAEL, as established previously, for 24 h ([Corte-Real et al., 2019](#); [Karas et al., 2019](#)). The exposure time was selected to maintain consistency between experiments and compare exposure endpoints. Additionally, these exposure times were selected specifically during rapid developmental time periods. At 24 h post exposure, larvae were manually dechorionated and fixed in 4% PFA for 2–4 h at RT. Samples were then PBS-T rinsed (2 \times s for 5 min with Phosphate Buffered Saline + 0.1% Tween-20 [PBS-T]) and permeabilized for 2 h in PBS + 2% Triton X100. After permeabilization, samples were PBS-T rinsed and subsequently stained at 250 nM of Acti-stain 555 phalloidin (Cytoskeleton, Inc, Denver, Colorado) for 1 h at RT protected from light. Samples were then destained overnight and stored in Vectashield Antifade Mounting Medium with DAPI (Vector Laboratories, Burlingame, California) until fluorescent confocal imaging. Z-stack images were taken on an Olympus FV1000MPE microscope (Olympus XLPlan N 25 \times objective NA 1.05) in $3\ \mu\text{m}$ step size. Z-stacks were compressed and ImageJ was used to evaluate cytoskeletal disruption. Ten somites were evaluated for fluorescent intensity and filament fragmentation anterior to the tapered end of the yolk sac. Additionally, the first somite anterior and distal to the tapered yolk was used to count the number of filaments. Three experimental replicates were conducted. During analysis, larvae without filaments were not considered outliers. Filament fragmentation and filaments per somite counts were conducted blind; $N = 21\text{--}31$.

In vitro P-gp efflux assay. The ability of LCR134 to inhibit rhodamine 123 (Rh123) efflux mediated by zebrafish Abcb4 or Abcb5 was examined by flow cytometry as described previously ([Robey et al., 2008](#)). Human embryonic kidney 293 (HEK293) cells, obtained from American Type Culture Collection (Manassas,

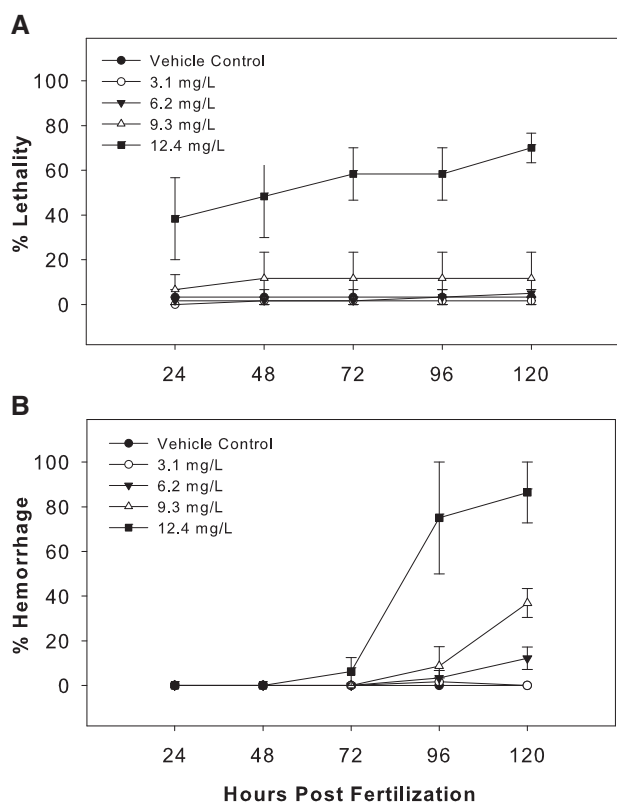


Figure 2. PMC79 daily observations. Four waterborne concentrations of PMC79 (3.1, 6.2, 9.3, and 12.4 mg/l) were used as exposure treatments in comparison to a 0.05% DMSO vehicle control over the course of 5 days. Lethality (A) and (B) hemorrhaging were measured cumulatively. Two experimental replicates were conducted, the ranges of which are displayed; $N = 60$.

Virginia), were transfected with empty vector, or vectors encoding zebrafish *abc4*, or *abc5*. MDR-19 cells that express human ABCB1 have been previously characterized (Robey et al., 2008). Cells were cultured in minimum essential medium (MEM), obtained from Mediatech (Manassas, Virginia), with 10% FBS, 1% glutamine, and 1% penicillin and expression was enforced by selection in 2 mg/ml G418 (Mediatech). For the efflux assay, cells were trypsinized, transferred to a 96-well round-bottom plate, resuspended in complete medium alone (phenol red-free MEM with 10% FBS, 1% glutamine, and 1% penicillin) or in complete medium with 0.5 μ g/ml Rh123 (Sigma-Aldrich), with or without the desired inhibitors—120 mg/l of the known human ABCB1 inhibitor cyclosporine A (CSA) (Sigma-Aldrich) or 1, 20, or 50 μ M LCR134 and incubated for 30 min at 37°C in 5% CO₂. Cells were subsequently washed, resuspended in substrate-free complete medium with or without inhibitors, and incubated for 1 h at 37°C in 5% CO₂. Cells were then washed with cold PBS and maintained on ice until analysis. Intracellular fluorescence was measured with a FACSCanto II flow cytometer (BD Biosciences,

San Jose, California). Rh123 was detected with a 488-nm argon laser with a 530-nm bandpass filter. At least 10 000 events were recorded for all samples. Histograms were generated using FlowJo software version 10.6.1 (Becton, Dickinson & Company, Franklin Lakes, New Jersey).

In vivo P-gp efflux assay. At 48 hpf, AB strain zebrafish embryos were manually dechorionated and treated with egg water with 0.05% DMSO vehicle, 120 mg/l CSA (Millipore, St Louis, Missouri) based on previous literature (Fischer et al., 2013), or at or below the LOAEL for LCR134. This time point was selected due to the high expression of the zebrafish P-gp homolog. All treatments contained at or below 0.05% of DMSO and 3 mg/l Rh123 (Millipore, St Louis, Missouri). Treatments were conducted in group housing with a maximum of 12 larvae; an $N = 4$ per dose. Free swimming larvae were rocked in the dark at RT for 2 h. Larvae were then rinsed in ice cold DI water, moved into fresh vials and rinsed again 3 \times s. After the final rinse larvae were transferred into microcentrifuge tubes, mechanically homogenized for 1 min and sonicated for 5 min. After sonication, samples were centrifuged with a quick spin, and aliquoted onto a black, clear bottom 96-well plate. The plate was read on a Varioskan LUX Fluorometer. The optics were directed from the bottom at excitation: 505 nm; emission: 530 nm with a bandwidth of 5 nm. Measurements were collected on SkanIt RE 6.0.2 software and were averaged as measurements from 29 points per well. Concentrations were calculated from a 10-point standard curve of Rh123 dissolved in egg water. Images were taken immediately after treatment and rinsing. Larvae were anesthetized in 0.01% MS-222 and imaged on a Zeiss Axio Observer 1 microscope with a X-Cite XFO 120 Light Source, Liquid Light Guide and Microscope Adapter and images were collected using ZEN 2 (Blue Edition) software. Three separate studies were conducted for a total $N = 11$ –12 per treatment.

Statistical analysis. Statistical analysis was conducted using SigmaPlot Version 11. *t* tests were conducted between positive and negative controls concurrently with a 1-way ANOVA in which metallodrugs were used at a single dose. For parametric and nonparametric data, 1-way ANOVA (post-hoc Holm-Sidak method) or Kruskal-Wallis 1-way analysis of variance on ranks (post-hoc Dunn's method) was used, respectively. Significance levels were set at $p < .05$.

RESULTS

PMC79 Treatment and Morphometric Analysis

The LOAEL doses for the metallodrugs were established for PMC79 as $0.17 \pm 1.7 \times 10^{-3}$ mg/l analytically determined Ru waterborne concentration and corresponding tissue dose 0.19 ± 0.05 Ru (ng/organism). LCR134 was established as $0.27 \pm 4.6 \times 10^{-2}$ mg/l analytically determined Ru waterborne concentration and corresponding tissue dose 0.30 ± 0.06 Ru (ng/organism).

Table 1. Morphometric Impacts of Three Anticancer Metallodrugs

	Total Body Length	Intraocular Distance	Yolk Sac Size	Pericardial Sac Size
Cisplatin (Karas et al., 2020)	(–)	(–)	(+)	NC
PMC79	(–)	(–)	(+)	NC
LCR134 (Corte-Real et al., 2019)	(–)	(–)	(+)	NC

NC, no change; (–), decreased; (+), increased. Morphometric measurements conducted for three metallodrugs, including total body length, intraocular distance, yolk sac size, and pericardial sac size indicated similar morphometric impact.

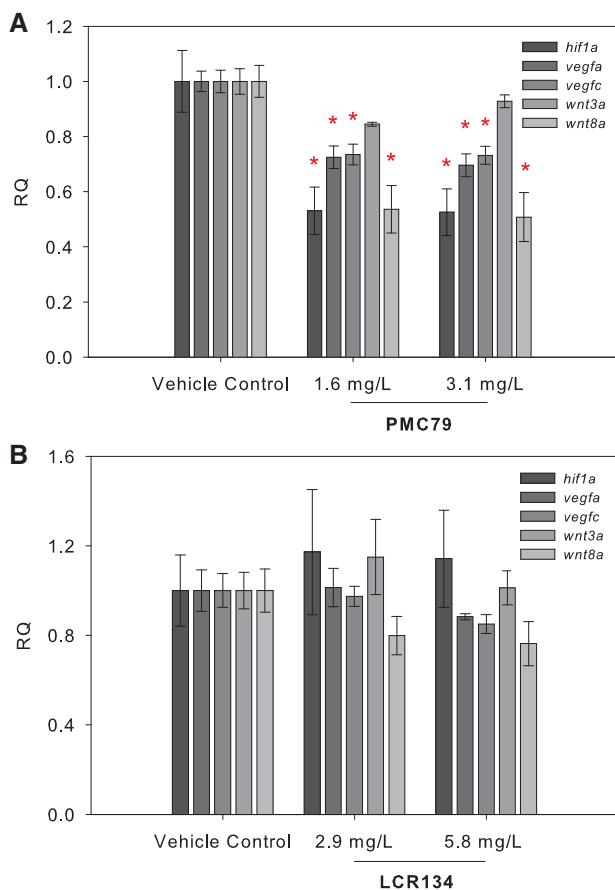


Figure 3. Gene Expression analysis. RNA transcript levels of genes for proliferation and angiogenesis were assessed after 24 h of exposure and included *hif1 α* , *vegfa*, *vegfc*, *wnt3a*, and *wnt8a*. Graphs represent the mean relative quantification (RQ) \pm the SEM of three experimental replicates ($N=3$). A 1-way ANOVA or Kruskal-Wallis ANOVA on ranks were used to determine a significant effect of metallo drugs PMC79 (A) and LCR134 (B) on transcript levels. An asterisk indicates a significant difference versus control as determined by Holm-Sidak or Dunn's post-hoc analyses ($p \leq .05$).

These data indicate that a LOAEL was established for LCR134 at approximately 1.5 fold higher than the waterborne and delivered tissue dose for PMC79.

Daily monitoring indicated that minimal lethality occurred at all but the highest dose (12.4 mg/l) of PMC79 (Figure 2A). In contrast, yolk sac edema was observed at all but the lowest dose (3.1 mg/l) and increased in the number of afflicted larvae after 72 hpf. Additionally, at or after 72 hpf, all but the lowest dose had hemorrhaging identified along the heart, DA, or posterior cardinal vein (PCV) with slowed heartbeats (Figure 2B). A significant dose-dependent decrease in total body length mirrored with a dose-dependent increase in yolk sac size after exposure to the 3 highest doses (nominal values: 6.2, 9.3, and 12.4 mg/l) of PMC79 was observed. A significant decrease in the intraocular distance of the highest three doses was observed, and although this was not dose dependent, the threshold dose of 3.1 mg/ml appeared to have a wider range of distribution than the top two doses. Lastly, pericardial sac did not appear to be significantly impacted by PMC79 exposure. Because lesions and/or lethality were observed at all doses, no NOAEL was established for PMC79.

Delayed hatching was not observed in PMC79 or LCR134 exposed embryos although it has been well established that cisplatin causes delay hatching in zebrafish in low doses with no lethality or additional lesions and, strikingly, up to 5 days post-fertilization (dpf). (Karas et al., 2019; 2020; Kovacs et al., 2016). Table 1 summarizes the morphometric endpoints observed in all 3 metallo drugs exposures. Each drug resulted in similar morphometric impacts including a decrease in total body length, and intraocular distance as well as an increase in yolk sac size. Although, PMC79 did not significantly alter pericardial sac size, it was the only compound tested that caused vascular damage.

Gene Expression

RNA transcript levels of several genes involved in proliferation and angiogenesis were measured after 24 h of exposure at or below the LOAELs of PMC79 and LCR134. Exposure to the parent compound PMC79, resulted in a significant decrease in all investigated genes (except *wnt3a*), with *hif1 α* and *wnt8a* as the most impacted at a ~ 0.5 -fold reduction. LCR134 exposure did not result in a significant alteration of gene expression in the pathway (Figure 3).

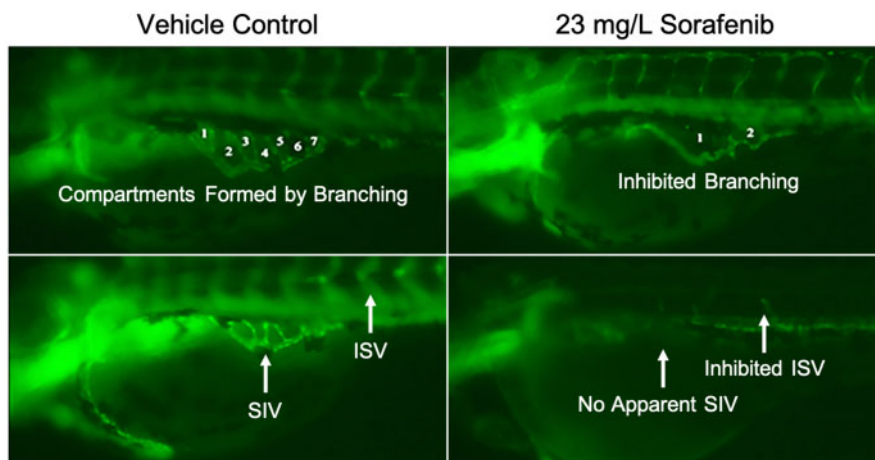


Figure 4. Zebrafish blood vessel inhibition. Exposure to the potent antiangiogenic compound sorafenib, caused severe inhibition of blood vessel development and branching. Numbers refer to the compartments formed by subintestinal interconnecting vessels or branching. Vehicle control organisms demonstrate normal subintestinal vessel (SIV) development as well as intersegmental vessels (ISV). Sorafenib treated larvae demonstrated inhibited branching, SIV, and ISV formation.

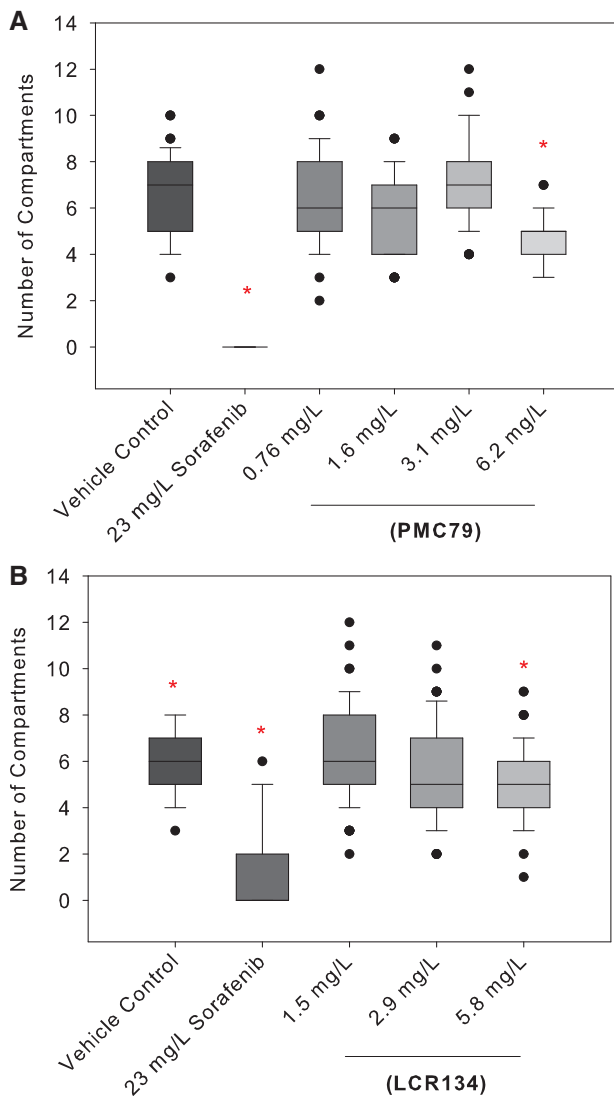


Figure 5. Basket branching. Live animal fluorescent imaging was conducted at 72 hpf. Graphs represent the average total number of compartments formed by subintestinal basket branching after exposure to 0.05% DMSO vehicle control, 23 mg/l sorafenib positive control, PMC79 (A) or LCR134 (B). The highest dose of PMC79 showed a 57% reduction in the average number of compartments. Kruskal-Wallis 1-way ANOVA on Ranks with Dunn's post hoc was used to determine significance; * indicates $p < .05$. Counts were taken using ImageJ software. $N = 39-80$. Experiments were conducted in triplicate.

Angiogenesis Impacts

Vascular insult was investigated by assessing SIV vessel length and corresponding area, number of interconnecting vessels (branching) within the SIV, and inhibition of blood vessel length extension from DA to dorsal lateral vein by an ISV to trunk width to vessel length ratio (Chimote et al., 2014; Delov et al., 2014; Serbedzija et al. 1999). In this study, we used sorafenib, a multikinase inhibitor that targets tumoral angiogenesis, and is used in the treatment of metastatic cancers. In almost all larval exposure to sorafenib, both SIV baskets and ISV blood vessels were severely inhibited or not formed (Figure 4). No significant blood vessel inhibition was found in the ISV vessels or decrease in basket area for either PMC79 or LCR134. However, PMC79 appeared to cause perturbations. The lowest dose of PMC79 caused an increase in basket area (data not shown), whereas the highest treated dose caused a 57% reduction in SIV basket

branching, while the highest dose of LCR134 caused a 17% reduction (Figure 5).

Tail Fin Regeneration

Cisplatin, PMC79, and LCR134 resulted in a significant reduction in the total area of regenerated tail fin compared with the cut control (Figure 6A). PMC79 and LCR134 exposure resulted in significantly less overall DAPI-labeled cells. Tail fins were additionally stained for proliferating cell nuclear antigen (PCNA) as a marker for cells undergoing proliferation. When PCNA was considered in terms of overall DAPI (PCNA/DAPI), exposure to each metallodrugs resulted in significantly less cell proliferation (Figs. 6B and 6C and 7).

P-gp Efflux Regulation

Inhibited transportation of Rh123 was assessed in human ABCB1 (P-gp), zebrafish Abcb4 and Abcb5 in vitro through flow cytometry analysis (Figure 8). HEK293 cells were transfected to derive human ABCB1 (P-gp), zebrafish Abcb4, and zebrafish Abcb5 expressing cell lines. Rh123 readily diffuses across the plasma membrane of cells, but is selectively effluxed by P-gp transporters. As such, accumulation of this fluorescent substrate indicates a lack of P-gp activity. The control group was treated with media only and no fluorescent signal was detected. The efflux group was treated with Rh123 only. At 120 mg/l, CSA, a known human P-gp inhibitor, caused accumulation of Rh123 in cells transfected with human P-gp as well as by zebrafish Abcb4 and Abcb5. LCR134 did not appear to have an effect on any of the transporters at 1.3 mg/l, whereas 25.8 mg/l was only partially effective on zebrafish Abcb4. At a concentration of 64.6 mg/l, LCR134 inhibited all of the transporters.

P-gp pump inhibition in the whole zebrafish was evaluated by the retention of the fluorescent substrate Rh123. CSA-treated larvae retained approximately twice the amount of Rh123 as control larvae (0.045 ± 0.012 and 0.026 ± 0.016 picomol/larvae), whereas 2-fold LOAEL treatments of LCR134 contained 7 and 44 \times s higher Rh123 compared to control: 0.181 ± 0.116 and 1.125 ± 0.420 picomol/larvae, respectively (Figure 9). The mRNA levels of the P-gp gene (*mdr1*) were analyzed in zebrafish treated with LCR134. Relative expression of this gene was unchanged after 24 h of exposure (data not shown).

Cytoskeletal Evaluation

Cytoskeletal disruption by PMC79 was evaluated by fluorescent intensity, filament fragment number, and filament number within the area of a somite (Figure 10). The 10 somites adjacent to the yolk extension were chosen in order to observe impacts on gradation of maturity due to anteroposterior development (Kimmel et al., 1995). Results indicated that 3.1 and 6.2 mg/l of PMC79 showed significant and proportional reduction in fluorescent intensity as the positive control, 1 mg/l Cytochalasin D (Figure 10A). This is in agreement with the number of filaments per somite area in which PMC79 (6.1 mg/l) and Cytochalasin D exposure caused a significant reduction in filament density (Figure 10B). However, Cytochalasin D exposure clearly caused a greater decrease compared with the negative control as opposed to the PMC79 at 6.1 mg/l (median values: 17, 2, and 14 filaments per $10^4 \mu\text{m}^2$ somite area; vehicle control, Cytochalasin D, and 6.1 mg/l PMC79, respectively).

The number of fragments within the 10 somites anterior to the tapering of the yolk sac were evaluated. Results demonstrated that Cytochalasin D had approximately twice the occurrence of fragments compared with the negative control

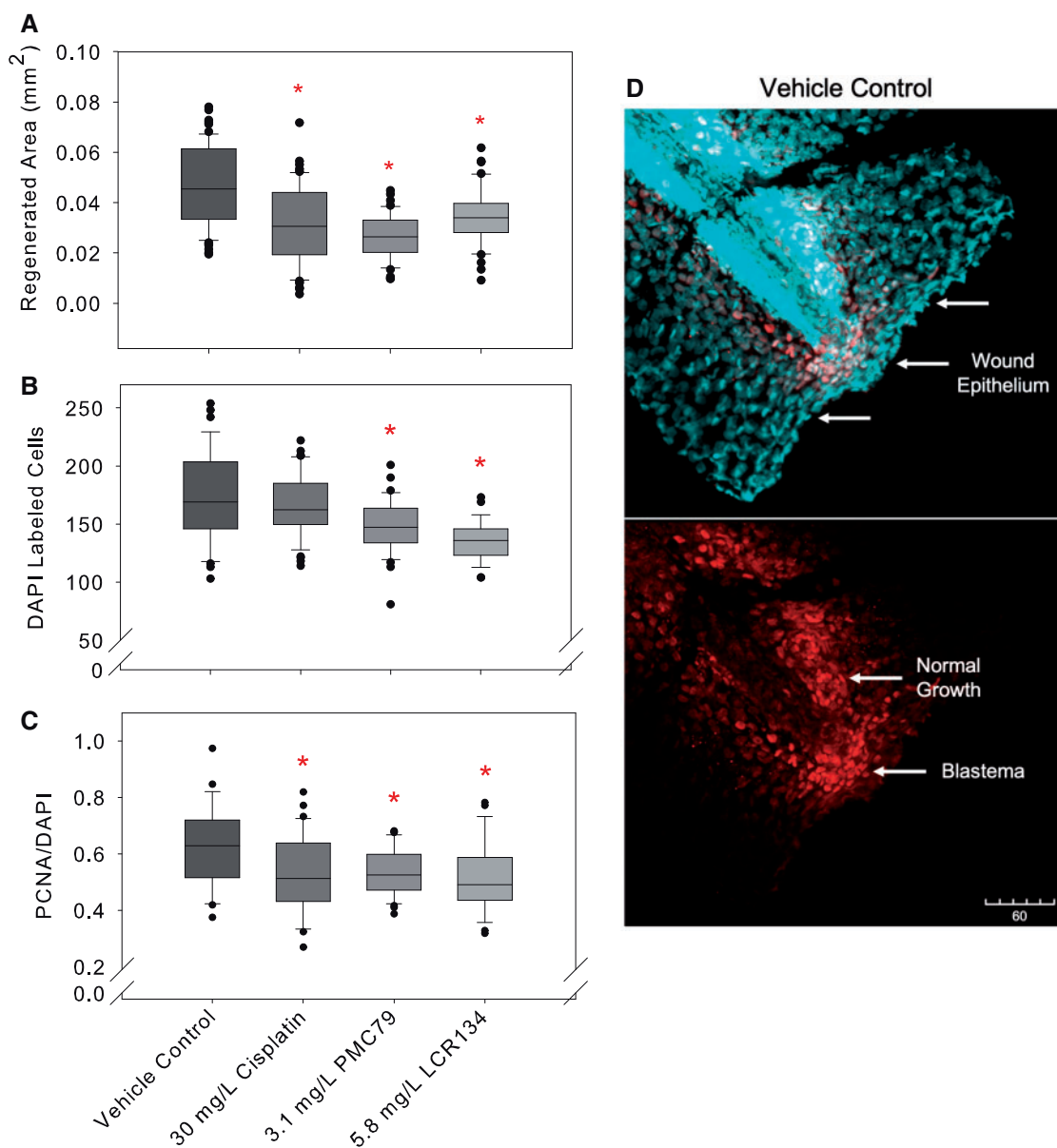


Figure 6. Caudal fin regeneration. Regeneration of caudal fins and whole mount fluorescent imaging was conducted after 24 h of regeneration in selected media: 0.05% DMSO vehicle control, 30 mg/l cisplatin positive control, 3.1 mg/l PMC79, and 5.8 mg/l LCR134. (A) Total area of regeneration after exposure to respective metallodrug or vehicle control (B) DAPI-stained cells (C) the relative number of PCNA to DAPI labeled cells. Kruskal-Wallis ANOVA on Ranks was used to determine a significant effect of metallodrugs. * indicates a significant difference analyses with post-hoc Dunn's method ($p \leq .05$). Counts were conducted using ImageJ software. Three experimental replicates were conducted: $N = 26-66$. (D) During wound repair tail fins begin to heal by forming a wound epithelium, depicted here as a dense area of cells along the point of amputation (upper image). Normal proliferative growth at the ventral posterior region occurs simultaneously as a blastema, or mass of proliferating mesenchymal cells, forms for regeneration (lower image). DAPI a cellular marker is stained as cyan and proliferating cell nuclear antigen (PCNA) a marker for proliferation is stained red.

(medians: 25 and 13 fragments per $10^4 \mu\text{m}$ somite area). Both doses of PMC79 showed a decrease in the number of fragments within this area compared with the negative control, although these data were not significant (median values: 13, 9, and 7, vehicle control, 3.1 and 6.2 mg/l PMC79, respectively) (Figure 10C). A visual comparison of the level of disorganization in the muscle myomeres caused by treatments can be seen in Figure 10D.

The mRNA levels of beta-actin were analyzed in zebrafish treated with 1.6 and 3.1 mg/l PMC79. Relative expression of this gene was significantly reduced after 24 h of exposure to both doses of the PMC79 metallodrug (Supplementary Figure 3).

DISCUSSION

Gross Morphological Impact

Morphometric analysis demonstrated that PMC79 and LCR134 exposure resulted in reduced total body length complementary with increased yolk sac size in a dose-dependent manner (Supplementary Figure 1). Neither Ru drugs caused delayed hatching, unlike cisplatin exposure which results in chorionic hardening and impaired hatching (Karas et al., 2020). All metallodrugs caused a reduction in total growth and proliferation which was mirrored by a reduction in nutrient uptake and distribution from the yolk (Corte-Real et al., 2019). In addition,

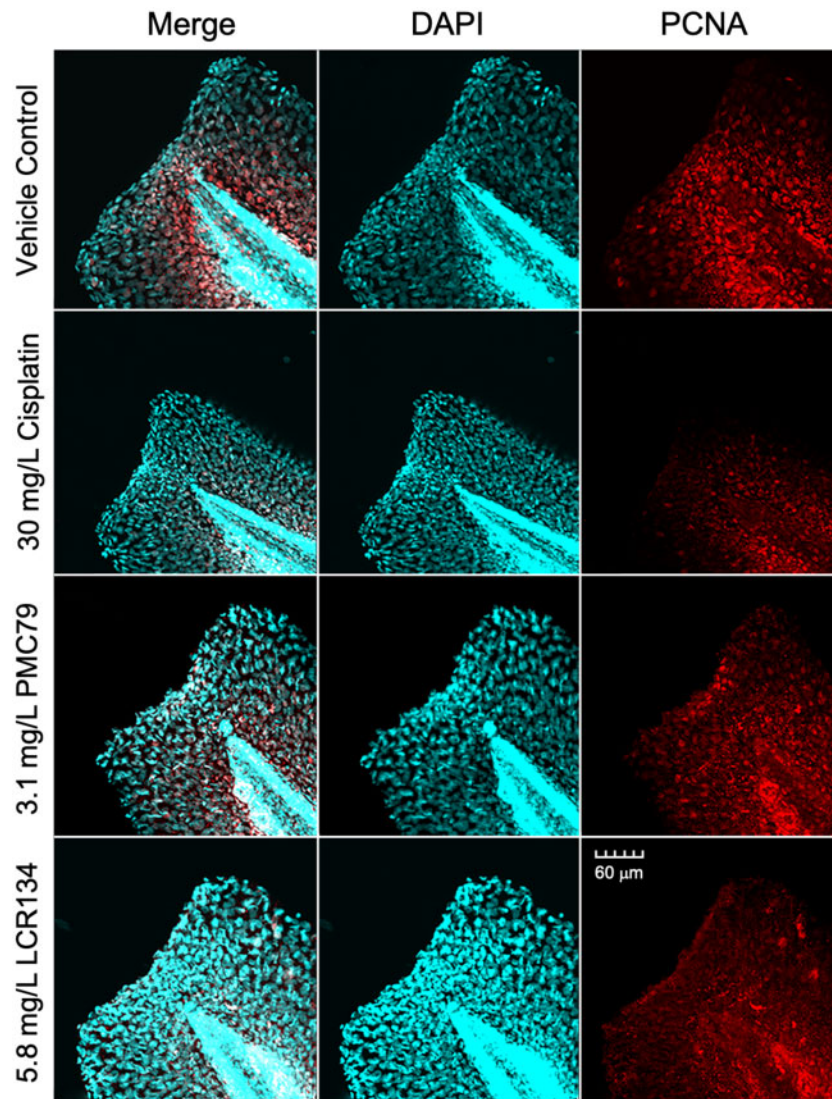


Figure 7. Immunofluorescent labeling. Whole mount fluorescent imaging was conducted after 24 h of regeneration in selected media: 0.05% DMSO vehicle control, 30 mg/l cisplatin positive control, 3.1 mg/l PMC79, and 5.8 mg/l LCR134. The first column depicts a merged image of PCNA and DAPI, whereas the second two columns depict DAPI and PCNA, respectively.

exposure to each metalldrugs resulted in a decrease in intraocular distance, indicating an impact on craniofacial development at higher doses in the developing organisms. These results could indicate impaired proliferation and migration of dividing cells. Furthermore, hemorrhaging identified after exposure to PMC79, but not in cisplatin or LCR134 indicates that these compounds may impact disparate pathways (Figure 2). The grossly observed lesions are likely a manifestation of one or multiple endpoints presented in the Results and discussed in the sections below. Impacting the cytoskeletal characteristics of the vascular endothelial cells, decreased VEGF/Hif pathway, decreased cell proliferation and altered transporters could explain the similarities and dissimilar lesions associated with PM79 and LCR134.

Antiproliferative and Angiogenic Properties

Whole organism antiproliferative properties observed by stunted growth were further evaluated by gene expression, blood vessel measurements, and tail fin regeneration. Although

both PMC79 and LCR134 impeded growth, development, and tail fin regeneration, gene transcription analysis demonstrated that PMC79 impacted the HIF-VEGF pathway at 24 hpf whereas LCR134 did not (Figure 3). As the parent compound of LCR134, PMC79 may be inducing its antiproliferative capabilities through a separate cellular pathway and this difference in gene regulation suggests that biotin is not cleaved from LCR134 giving rise to its parental structure during interaction with the cell. This is supported by a unique hemorrhaging lesion observed after the 3 highest doses of PMC79 exposure (Figure 2) and localized near the DA, as well as 57% inhibition in basket branching within the SIV at the lowest dose: 3.1 mg/l (Figure 5). Sorafenib exposure in developing zebrafish embryos caused a near inhibition of blood vessels within the trunk as well as the yolk sac (Figs. 4 and 5). This was almost always visualized with significant pericardial sac edema and is commonly associated with VEGFR inhibitors in zebrafish as well as clinically (Chimote et al., 2014; Chu et al., 2007). However, treatment of PMC79 resulted in specific impact to the SIV without pericardial sac or ISV insult (Figs. 9–11). SIVs

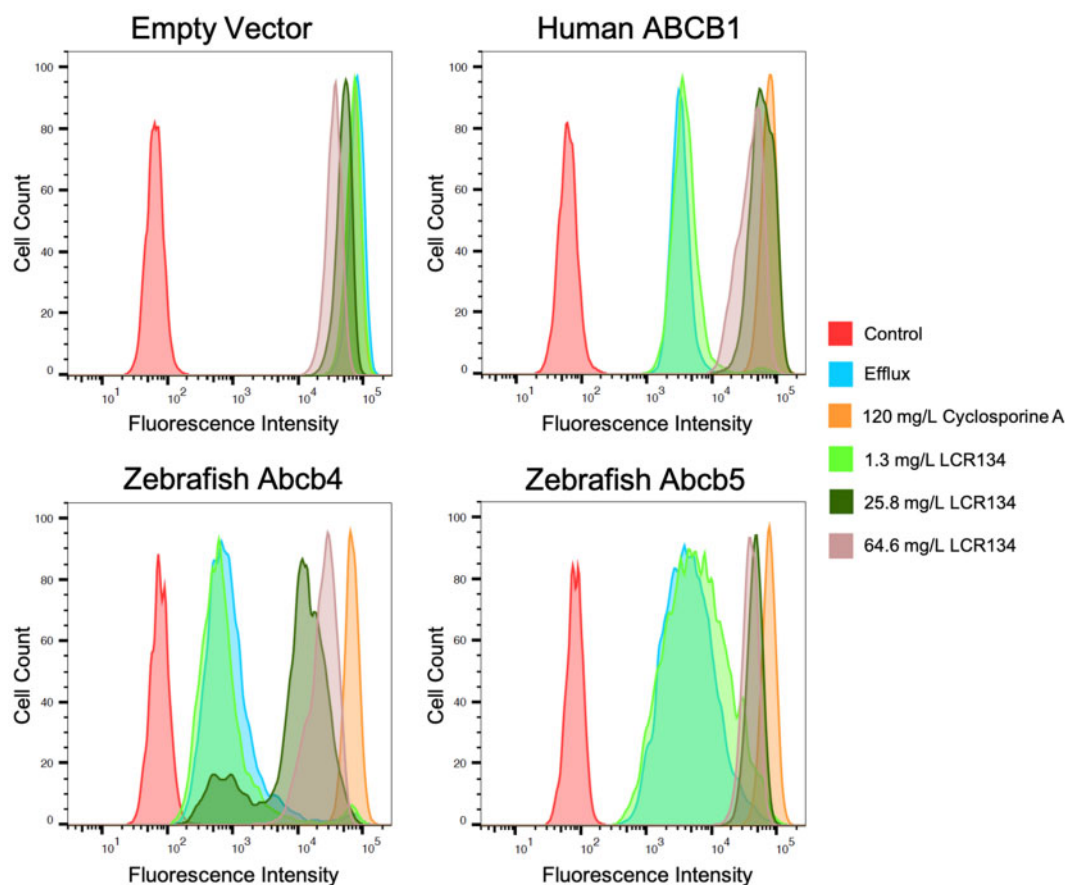


Figure 8. In vitro inhibition of P-gp orthologous zebrafish transporters. Human embryonic kidney 293 (HEK293) cells were transfected with an empty vector, or vectors encoding human ABCB1, zebrafish *abcb4*, or *abcb5*. For the efflux assay, cells were resuspended in complete medium alone or in complete medium with 0.5 g/ml Rh123 with or without the desired inhibitors: 120 mg/l cyclosporine A (CSA), or 1.3, 25.8, 64.6 mg/l LCR134. Intracellular fluorescence was measured with a FACSCanto II flow cytometer. Rh123 was detected with a 488 nm argon laser with a 530-nm bandpass filter. At least 10 000 events were recorded for all samples. Histograms were generated using FlowJo software version 10.6.1.

are outgrowths of the PCV and subsequently form a plexus with organized branching, whereas the ISVs are a retained primary structure (Childs *et al.*, 2002). Although there are regional differences in angiogenesis signaling and physiology, sorafenib was able to inhibit both ISVs and SIVs, most likely due to its nonspecific kinase targeting. However, PMC79 appears to specifically cause insult during the organization branching of the subintestinal plexus. Here the zebrafish model was able to elucidate distinct regional angiogenic impacts that would have been unable to be observed without the context of in vivo heterogeneity. Although alternative in vivo angiogenic assays exist, such as the matrigel plug and chick chorioallantoic membrane assays they are limited by their throughput capacity. Given the distinction in results, it is important for future studies of novel compounds to evaluate both regions of blood vessels due to potential targeting selectivity.

The doses selected for tail fin regeneration coupled with immunofluorescent staining were based off the 5-day dose response LOAEL PMC79 and LCR134 concentrations. However, the cisplatin dose was selected at the established 5-day LC₅₀, which demonstrated minimal lethality for a 24-h exposure. Although cisplatin exposure was conducted at a more toxic dose, exposure to each of the three metallodrugs demonstrated similar reduction in total area of regeneration and reduced PCNA signaling for proliferation (Figure 6). This complemented with cell culture IC₅₀ results demonstrating increased sensitivity to

the Ru drugs compared with cisplatin (Corte-Real *et al.*, 2019). In addition, a study conducted by Wang *et al.*, in 2009 demonstrated novel Ru drugs resulted in PCNA downregulation and a significant caudal fin-reduction phenotype compared with cisplatin and were less toxic, although fins in this study were not amputated. This suggests that the Ru drugs enact their antiproliferative capabilities comparatively to cisplatin with the advantage of being well below a lethal endpoint. Additionally, PMC79 and LCR134, unlike cisplatin, did not appear to impact normal cell proliferation at the ventral posterior region which form independently of injury as previously demonstrated by Kawakami *et al.* in 2004 and confirmed in our studies as shown in Figure 17. The alkylating activity of cisplatin is unable to distinguish cancerous and normal proliferating cells, however, PMC79 and LCR134 show distinct targeting during tail fin regeneration studies. The repair of an epithelial wound involves transient activation of cellular mechanisms alongside proliferation including inflammatory response, angiogenesis, cellular migration, and tissue matrix remodeling (Erming *et al.*, 2014). Due to differences in downregulation of normal and injury induced PCNA after metallodrugs treatment, Ru drugs may be more selectively targeting signaling involved in these mechanisms.

PMC79 and LCR134 In Vivo Mechanistic Activity

We previously demonstrated that LCR134 inhibits human P-gp in vitro (Corte-Real *et al.*, 2019), and although the zebrafish does

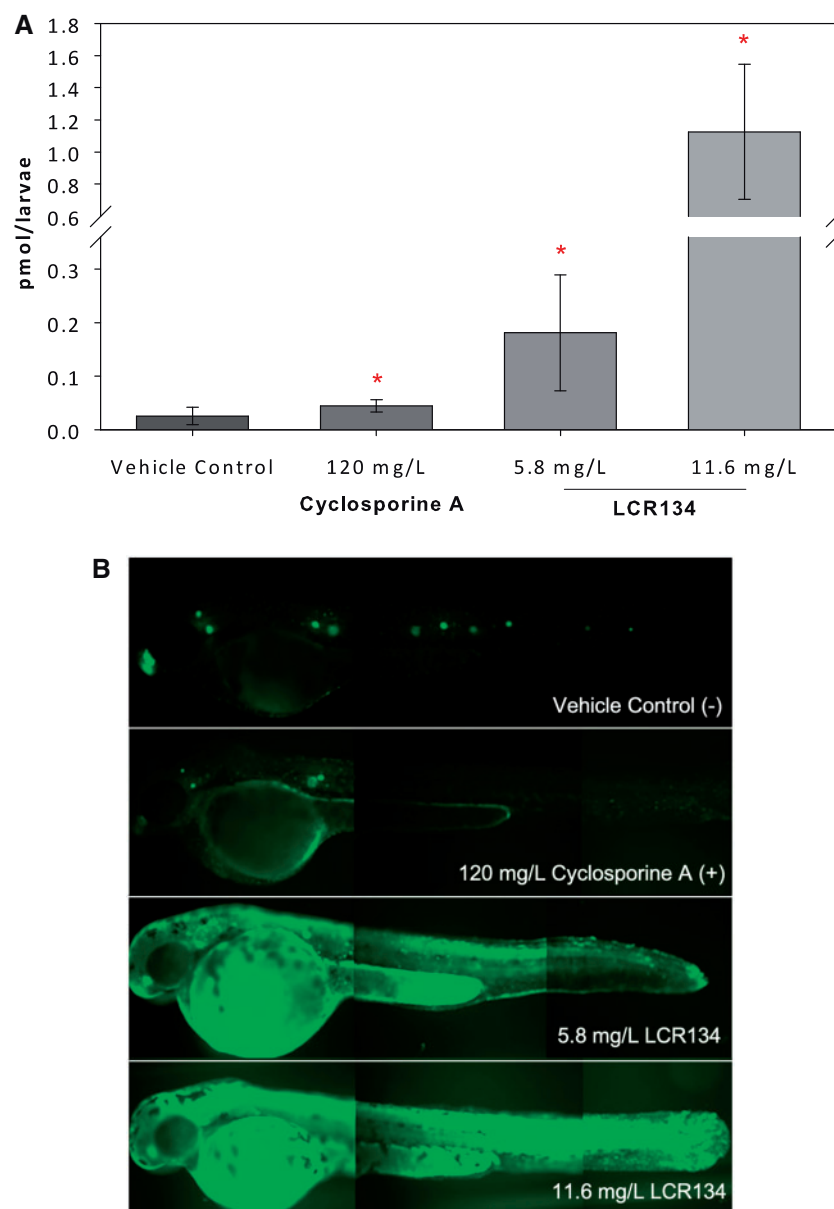


Figure 9. P-gp inhibition. Free-swimming larvae at 48 hours postfertilization (hpf) were co-incubated with Rh123, a fluorescent P-gp substrate, and vehicle control (-), 120 mg/l CSA (+), 5.8 mg/l LCR134, or 11.6 mg/l LCR134 and a cohort subsequently imaged (B). Larval tissue was analyzed using a Varioskan LUX Fluorometer. Optics were directed from the bottom at excitation: 505 nm; emission: 530 nm with 5 nm bandwidth. Asterisks indicate significant difference from the control: $p < .05$. A t test was conducted between the two controls and Kruskal-Wallis 1-way ANOVA, with post-hoc Dunn's method was conducted for the control and two doses of LCR134. Three experimental replicates were conducted; $N = 11-12$.

not express a direct homolog of ABCB1, the gene that encodes for human P-gp, it does express two genes that have similar function, *abcb4* and *abcb5* (Fischer et al., 2013). This led us to examine the effects of LCR134 on Rh123 efflux from cells transfected to express zebrafish *Abcb4* or *Abcb5* as well as cells expressing human P-gp. LCR134 demonstrated an ability to inhibit the multidrug resistant P-gp transporter across species in vitro supporting pharmacological translatability. In the whole organism model, larvae treated with LCR134 showed a dose dependent increase in the amount of accumulated P-gp substrate, Rh123, during a 2-h exposure both quantitatively and qualitatively (Figure 9). Unexpectedly, LCR134 showed a marked increase in accumulation compared with CSA, even at levels

below the 120 h LOEL exposure dose established in zebrafish larvae. Additionally, *mdr1* mRNA transcript levels of embryos exposed for 24 h were unaffected, further supporting a form of protein inhibition. The potency at which LCR134 inhibits P-gp transporters may suggest the clinical efficacy at very low doses, potentially limiting off-target effects and increasing compatibility with coadministered chemotherapeutics. Because this transporter is responsible for removing drugs from sites of action, the upregulation of these transporters in cancer cells is correlated with poor prognosis and remains a limitation for chemotherapeutic treatment (Chung et al., 2016). Specifically, the inhibition of this pump in zebrafish could have translational relevance for overcoming chemotherapeutic resistance. In

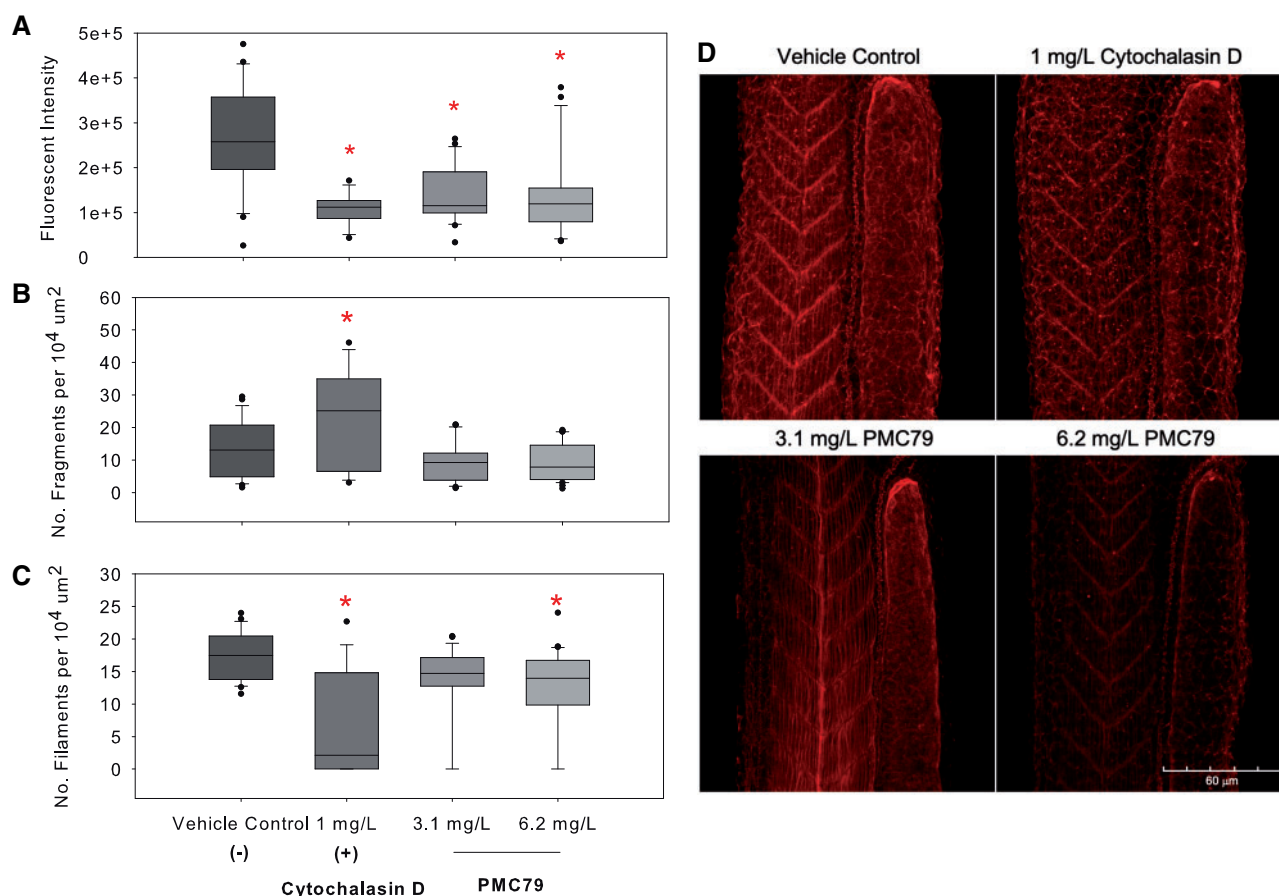


Figure 10. Cytoskeletal evaluation. Zebrafish Larvae were exposed to vehicle control (A), 1 mg/l Cytochalasin D (B), 2.9 mg/l PMC79 (C), and 5.8 mg/l PMC79 (D) and subsequently fixed and stained with phalloidin. Fluorescent intensity (top), number of fragments (middle), and number of filaments per $10^4 \mu\text{m}^2$ somite area (bottom) were evaluated. *t* tests were run between positive and negative controls. Kruskal-Wallis 1-way analysis were conducted with post-hoc Dunn's method. Asterisks indicate significance at $p < .05$. Experiments were run in triplicate, $N = 21-31$. Zebrafish Larvae were exposed to vehicle control (A), Cytochalasin D (B), 2.9 mg/l PMC79 (C), and 5.8 mg/l PMC79 (D) and subsequently fixed and stained with phalloidin. Stacked images were taken on an Olympus FV1000MPE microscope (Olympus XLPlan N 25x objective NA 1.05) in $3 \mu\text{m}$ step size. Z-stacks were compressed and ImageJ was used to evaluate cytoskeletal disruption.

future studies, the compatibility and drug interaction of LCR134 with cisplatin and additional P-gp effluxed chemotherapeutics should be investigated.

Although PMC79 is the parental compound of LCR134, the *in vivo* activity was dissimilar. Cytoskeletal impacts, that is the depolymerization of F-actin observed *in vitro*, were investigated in the zebrafish model. PMC79 significantly decreased the fluorescent intensity quantified within the somites of the fish in addition to increased disorganization. This was in agreement with a decrease in the number of filaments assessed per somite area (Figure 10). Overall, this suggests a decrease in the density of cytoskeleton within the area adjacent to the yolk extension. The number of fragments caused by disruption of cytoskeletal development was also assessed. Significance was found between the vehicle control and cytochalasin D, which binds to the end of F-actin preventing the addition of new monomers (Cooper, 1987). However, PMC79 exposure did not cause an increase in fragment number. This may be due to a different mechanism of cytoskeletal impact in which PMC79 is depolymerizing and reducing the overall number of filaments and therefore fragmentation sites. Additionally, zebrafish mRNA transcript levels of beta-actin were significantly reduced at both PMC79 exposure doses (Supplementary Figure 3). Beta-actin is responsible for the

maintenance of total actin and regulation of the cellular G-actin concentration (F-actin monomer), and as such may be interfering with actin formation signaling pathways (Bunnell *et al.*, 2011). Cytoskeleton inhibitors are a class of anticancer compounds, but not without inherent issues. Compound differentiation between healthy and cancerous cells continues to be a challenge, as actin cytoskeleton is essential for cell function. In these studies, previously established LOAEL doses based on morphometric evaluation were able to decrease cytoskeleton density. However, the zebrafish larvae are a particular sensitive model for cytoskeleton toxicity due to active development. Further studies are warranted in adult organisms for off-target toxicity and specificity.

Zebrafish show great promise as an asset to pharmacology and toxicology and do well to complement the drug development paradigm. These studies suggest that the zebrafish can be utilized to study novel metallodrugs and can include lead discovery, modes of action, target identification, and toxicological studies. Although the zebrafish model has been limited due to the difficulties in determining drug uptake due to waterborne treatments, our previous bioanalytical work applying ICP-MS quantification for metallodrugs overcomes this. To conclude, the zebrafish serves as a highly applicable model to investigate metallodrugs in the context of a whole organism.

Summary

PMC79 and LCR134 are next-generation Ru-based metallodrugs. Ru-based drug candidates were designed with the intent to improve upon the broad spectrum and resulting off-target toxicity of cisplatin. In this study, we showed two Ru drugs with anti-proliferative capacity at doses at or below established LOAELs with comparative capacity at toxic doses of cisplatin in the zebrafish model. We also established that PMC79 may have antiangiogenic capabilities specific for areas of blood vessel remodeling which may be pertinent to the tumor microenvironment. However, careful consideration of this model for blood vessel functionality, not just inhibited formation, should be taken, considering developmental zebrafish survivability in the absence of blood vessels by passive oxygen diffusion (Wilkinson and van Eeden, 2014). In conclusion, PMC79 and LCR134 show promising anticancer properties and warrant further investigation into higher vertebrate models.

Future studies could examine zebrafish tumor xenograft screening. These screenings have shown to be useful in elucidating solid tumor proliferation, tumor inducible neovascularization, and cancer cell invasion (Ren et al., 2017; Lee et al., 2009; Marques et al., 2009; Nicoli et al., 2007). Recently, the zebrafish tumor xenograft screening tool has been exploited in personalized medicine for patient specific efficacious drugs (Veinotte et al., 2014). Given the heterogeneity of cancers, the success of these screening xenografts could by-pass patient chemotherapeutic trial and error which result adverse side effects and lower quality of life. These studies have shown promising antiproliferative potential of Ru metallodrugs in a higher throughput in vivo model. Although, the mechanisms by which these compounds act are still unknown, the zebrafish have shown to be a successful platform in elucidating relative efficacy and toxicity of novel Ru metallodrugs.

SUPPLEMENTARY DATA

Supplementary data are available at Toxicological Sciences online.

ACKNOWLEDGMENTS

We state our appreciation for Dr Huaye Zhang for use of the confocal microscope, Drs Lori A. White, Kyle Murphy, and Phoebe Stapleton for their guidance on this research. We also thank the following dedicated undergraduate researchers: Saul Abreu, Michelle Bilotti, Sameh Melhem, Danielle Slomko, June White, and Cassie Winz.

FUNDING

New Jersey Agricultural Experiment Station (NJAES)-Rutgers (NJ01201 to B.F.K.), and National Institute of Environmental Health Sciences (NIEHS) Training (T32-ES 007148 to B.F.K.); FCT PhD (SFRH/BD/100515/2014 to L.C.-R.) and Fulbright Research (2017/2018 with the support of Portuguese Foundation for Science and Technology / Fundação para a Ciência e Tecnologia (FCT) to L.C.-R.); National Institutes of Health-NIEHS (P30 ES005022 to B.T.B.); NJAES Project 01202 (W2045 to K.R.C.), and National Institutes of Health (ES005022 to K.R.C.); Portuguese Foundation for Science and Technology (Fundação para a Ciência e Tecnologia, FCT) for Projects (UIDB/00100/2020, PTDC/QUI-QIN/28662/2017 to

A.V.) and the CEEC Individual 2017 (CEECIND/01974/2017 to A.V.); National Institutes of Health Institutional Research and Career Development Award (IRACDA) (1K12GM093854 to V.D.).

DECLARATION OF CONFLICTING INTERESTS

The authors declared no potential conflicts of interest with respect to the research, authorship, and/or publication of this article.

REFERENCES

- Abid, M., Shamsi, F., and Azam, A. (2016). Ruthenium complexes: An emerging ground to the development of metallopharmaceuticals for cancer therapy. *Mini Rev. Med. Chem.* **16**, 772–786.
- Alessio, E., and Messori, L. (2019). Nami-a and kp1019/1339, two iconic ruthenium anticancer drug candidates face-to-face: A case story in medicinal inorganic chemistry. *Molecules* **24**, 1995.
- Alessio, E., Mestroni, G., Bergamo, A., and Sava, G. (2004). Ruthenium antimetastatic agents. *Curr. Top. Med. Chem.* **4**, 1525–1535.
- Ren, J., Liu, S., Cui, C., and ten Dijke, P. (2017). Invasive behavior of human breast cancer cells in embryonic zebrafish. *JoVE* **122**, e55459.
- Baba, Y., Noshio, K., Shima, K., Irahara, N., Chan, A. T., Meyerhardt, J. A., Chung, D. C., Giovannucci, E. L., Fuchs, C. S., and Ogino, S. (2010). Hif1a overexpression is associated with poor prognosis in a cohort of 731 colorectal cancers. *Am. J. Pathol.* **176**, 2292–2301.
- Bunnell, T. M., Burbach, B. J., Shimizu, Y., and Ervasti, J. M. (2011). B-actin specifically controls cell growth, migration, and the g-actin pool. *Mol. Biol. Cell* **22**, 4047–4058.
- Burris, H. A., Bakewell, S., Bendell, J. C., Infante, J., Jones, S. F., Spigel, D. R., Weiss, G. J., Ramanathan, R. K., Ogden, A., and Von, H. D. (2016). Safety and activity of IT-139, a ruthenium-based compound, in patients with advanced solid tumours: A first-in-human, open-label, dose-escalation phase I study with expansion cohort. *ESMO Open* **1**, e000154.
- Campbell, E. J., Dachs, G. U., Morrin, H. R., Davey, V. C., Robinson, B. A., and Vissers, M. C. M. (2019). Activation of the hypoxia pathway in breast cancer tissue and patient survival are inversely associated with tumor ascorbate levels. *BMC Cancer* **19**, 307.
- Chen, L., Shi, Y., Yuan, J., Han, Y., Qin, R., Wu, Q., Jia, B., Wei, B., Wei, L., Dai, G., et al. (2014). Hif-1 alpha overexpression correlates with poor overall survival and disease-free survival in gastric cancer patients post-gastrectomy. *PLoS One* **9**, e90678.
- Chen, S., Zhao, X., Chen, J., Chen, J., Kuznetsova, L., Wong, S. S., and Ojima, I. (2010). Mechanism-based tumor-targeting drug delivery system. Validation of efficient vitamin receptor-mediated endocytosis and drug release. *Bioconj. Chem.* **21**, 979–987.
- Childs, S., Chen, J.-N., Garrity, D. M., and Fishman, M. C. (2002). Patterning of angiogenesis in the zebrafish embryo. *Development* **129**, 973–982.
- Chimote, G., Sreenivasan, J., Pawar, N., Subramanian, J., Sivaramakrishnan, H., and Sharma, S. (2014). Comparison of effects of anti-angiogenic agents in the zebrafish efficacy-toxicity model for translational anti-angiogenic drug discovery. *Drug Des. Dev. Ther.* **8**, 1107–1123.

- Chu, T. F., Rupnick, M. A., Kerkela, R., Dallabrida, S. M., Zurakowski, D., Nguyen, L., Woulfe, K., Pravda, E., Cassiola, F., Desai, J., et al. (2007). Cardiotoxicity associated with tyrosine kinase inhibitor sunitinib. *Lancet* **370**, 2011–2019.
- Chung, F. S., Santiago, J. S., Jesus, M. F. M. D., Trinidad, C. V., and See, M. F. E. (2016). Disrupting p-glycoprotein function in clinical settings: What can we learn from the fundamental aspects of this transporter? *Am. J. Cancer Res.* **6**, 1583–1598.
- Cooper, J. A. (1987). Effects of cytochalasin and phalloidin on actin. *J. Cell Biol.* **105**, 1473–1478.
- Côrte-Real, L., Karas, B., Brás, A. R., Pilon, A., AVECILLA, F., Marques, F., Preto, A., Buckley, B. T., Cooper, K. R., Doherty, C., et al. (2019). Ruthenium-cyclopentadienyl bipyridine-biotin based compounds: Synthesis and biological effect. *Inorg. Chem.* **58**, 9135–9149.
- Corte-Real, L., Karas, B., Girio, P., Moreno, A., AVECILLA, F., Marques, F., Buckley, B. T., Cooper, K. R., Doherty, C., Falson, P., et al. (2019). Unprecedented inhibition of p-gp activity by a novel ruthenium-cyclopentadienyl compound bearing a bipyridine-biotin ligand. *Eur. J. Med. Chem.* **163**, 853–863.
- Cunha, V., Burkhardt-Medicke, K., Wellner, P., Santos, M. M., Moradas-Ferreira, P., Luckenbach, T., and Ferreira, M. (2017). Effects of pharmaceuticals and personal care products (PPCPs) on multidrug resistance (MDR) related efflux transporter activity in zebrafish (*Danio rerio*) embryos. *Ecotoxicol. Environ. Saf.* **136**, 14–23.
- Delov, V., Muth-Köhne, E., Schäfers, C., and Fenske, M. (2014). Transgenic fluorescent zebrafish *tg(fli1: egfp)y1* for the identification of vasotoxicity within the zft. *Aquat. Toxicol.* **150**, 189–200.
- Eming, S. A., Martin, P., and Tomic-Canic, M. (2014). Wound repair and regeneration: Mechanisms, signaling, and translation. *Sci. Transl. Med.* **6**, 265sr266.
- Fischer, S., Kluver, N., Burkhardt-Medicke, K., Pietsch, M., Schmidt, A. M., Wellner, P., Schirmer, K., and Luckenbach, T. (2013). Abcb4 acts as multidrug transporter and active barrier against chemical uptake in zebrafish (*Danio rerio*) embryos. *BMC Biol.* **11**, 69.
- Fouquet, B., Weinstein, B. M., Serluca, F. C., and Fishman, M. C. (1997). Vessel patterning in the embryo of the zebrafish: Guidance by notochord. *Dev. Biol.* **183**, 37–48.
- Hall, M. D., Okabe, M., Shen, D. W., Liang, X. J., and Gottesman, M. M. (2008). The role of cellular accumulation in determining sensitivity to platinum-based chemotherapy. *Annu. Rev. Pharmacol. Toxicol.* **48**, 495–535.
- Karas, B. F., Côrte-Real, L., Doherty, C. L., Valente, A., Cooper, K. R., and Buckley, B. T. (2019). A novel screening method for transition metal-based anticancer compounds using zebrafish embryo-larval assay and inductively coupled plasma-mass spectrometry analysis. *J. Appl. Toxicol.* **39**, 1173–1180.
- Karas, B. F., Hotz, J. M., Buckley, B. T., and Cooper, K. R. (2020). Cisplatin alkylating activity in zebrafish causes resistance to chorionic degradation and inhibition of osteogenesis. *Aquat. Toxicol.* **229**, 105656.
- Kimmel, C. B., Ballard, W. W., Kimmel, S. R., Ullmann, B., and Schilling, T. F. (1995). Stages of embryonic development of the zebrafish. *Dev. Dyn.* **203**, 253–310.
- Kovacs, R., Bakos, K., Urbanyi, B., Kovesi, J., Gazsi, G., Csepeli, A., Appl, A. J., Bencsik, D., Csenki, Z., and Horvath, A. (2016). Acute and sub-chronic toxicity of four cytostatic drugs in zebrafish. *Environ. Sci. Pollut. Res. Int.* **23**, 14718–14729.
- Lee, S. L. C., Rouhi, P., Jensen, L. D., Zhang, D., Ji, H., Hauptmann, G., Ingham, P., and Cao, Y. (2009). Hypoxia-induced pathological angiogenesis mediates tumor cell dissemination, invasion, and metastasis in a zebrafish tumor model. *Proc. Natl. Acad. Sci. U.S.A.* **106**, 19485–19490.
- Leijen, S., Burgers, S. A., Baas, P., Pluim, D., Tibben, M., van Werkhoven, E., Alessio, E., Sava, G., Beijnen, J. H., and Schellens, J. H. (2015). Phase I/II study with ruthenium compound NAMI-A and gemcitabine in patients with non-small cell lung cancer after first line therapy. *Invest. New Drugs* **33**, 201–214.
- Leonard, I. Z., and Randall, T. P. (2005). In vivo drug discovery in the zebrafish. *Nat. Rev. Drug Discov.* **4**, 35.
- Liang, D., Chang, J., Chin, A., Smith, A., Kelly, C., Weinberg, E., and Ge, R. (2001). The role of vascular endothelial growth factor (VEGF) in vasculogenesis, angiogenesis, and hematopoiesis in zebrafish development. *Mech. Dev.* **108**, 29–43.
- Lieberthal, W., Triaca, V., and Levine, J. (1996). Mechanisms of death induced by cisplatin in proximal tubular epithelial cells: Apoptosis vs. necrosis. *Am. J. Physiol. Renal Physiol.* **270**, F700–F708.
- Lin, K., Zhao, Z.-Z., Bo, H.-B., Hao, X.-J., and Wang, J.-Q. (2018). Applications of ruthenium complex in tumor diagnosis and therapy. *Front. Pharmacol.* **9**, 1323–1323.
- Lipponer, K. G., Vogel, E., and Keppler, B. K. (1996). Synthesis, characterization and solution chemistry of trans-indazoliumtetrachlorobis(indazole)ruthenate(III), a new anticancer ruthenium complex. IR, UV, NMR, HPLC investigations and antitumor activity. Crystal structures of trans-1-methyl-indazoliumtetrachlorobis-(1-methylindazole)ruthenate(III) and its hydrolysis product trans-monoaquatrichlorobis-(1-methylindazole)-ruthenate(III). *Met. Based Drugs* **3**, 243–260.
- Maes, J., Verlooy, L., Buenafe, O. E., de Witte, P. A. M., Esguerra, C. V., and Crawford, A. D. (2012). Evaluation of 14 organic solvents and carriers for screening applications in zebrafish embryos and larvae. *PLoS One* **7**, e43850.
- Marques, I. J., Weiss, F. U., Vlecken, D. H., Nitsche, C., Bakkers, J., Lagendijk, A. K., Partecke, L. I., Heidecke, C. D., Lerch, M. M., and Bagowski, C. P. (2009). Metastatic behaviour of primary human tumours in a zebrafish xenotransplantation model. *BMC Cancer* **9**, 128.
- Moreira, T., Francisco, R., Comsa, E., Duban-Deweer, S., Labas, V., Teixeira-Gomes, A.-P., Combes-Soia, L., Marques, F., Matos, A., Favrelle, A., et al. (2019). Polymer “ruthenium-cyclopentadienyl” conjugates—New emerging anti-cancer drugs. *Eur. J. Med. Chem.* **168**, 373–384.
- National Cancer Institute. (2014). The “accidental” cure—Platinum-based treatment for cancer: The discovery of cisplatin. <https://www.cancer.gov/research/progress/discovery/cisplatin>. Accessed December 10, 2020.
- Nicoli, S., Ribatti, D., Cotelli, F., and Presta, M. (2007). Mammalian tumor xenografts induce neovascularization in zebrafish embryos. *Cancer Res.* **67**, 2927–2931.
- Noffke, A. L., Habtemariam, A., Pizarro, A. M., and Sadler, P. J. (2012). Designing organometallic compounds for catalysis and therapy. *Chem. Commun.* **48**, 5219–5246.
- OECD. (2013). Test no. 236: Fish embryo acute toxicity (FET) test. OECD guidelines for the testing of chemicals. <https://www.oecd-ilibrary.org/content/publication/9789264203709-en>. Accessed December 10, 2020.
- Pluchino, K. M., Hall, M. D., Goldsborough, A. S., Callaghan, R., and Gottesman, M. M. (2012). Collateral sensitivity as a strategy against cancer multidrug resistance. *Drug Resist. Updates* **15**, 98–105.
- Ren, W., Han, J., Uhm, S., Jang, Y., Kang, C., Kim, J.-H., and Kim, J. (2015). Recent development of biotin conjugation in

- biological imaging, sensing, and target delivery. *Chem. Commun.* **51**, 10403–10418.
- Robey, R. W., Shukla, S., Finley, E. M., Oldham, R. K., Barnett, D., Ambudkar, S. V., Fojo, T., and Bates, S. E. (2008). Inhibition of p-glycoprotein (abcb1)- and multidrug resistance-associated protein 1 (abcc1)-mediated transport by the orally administered inhibitor, CBT-1((R)). *Biochem. Pharmacol.* **75**, 1302–1312.
- Santoriello, C., and Zon, L. I. (2012). Hooked! Modeling human disease in zebrafish. *J. Clin. Invest.* **122**, 2337–2343.
- Serbedzija, G. N., Flynn, E., and Willett, C. E. (1999). Zebrafish angiogenesis: A new model for drug screening. *Angiogenesis* **3**, 353–359.
- Shaffer, B. C., Gillet, J.-P., Patel, C., Baer, M. R., Bates, S. E., and Gottesman, M. M. (2012). Drug resistance: Still a daunting challenge to the successful treatment of AML. *Drug Resist. Updates* **15**, 62–69.
- Shi, J.-F., Wu, P., Jiang, Z.-H., and Wei, X.-Y. (2014). Synthesis and tumor cell growth inhibitory activity of biotinylated annonaceous acetogenins. *Eur. J. Med. Chem.* **71**, 219–228.
- Tan, J. L., and Zon, L. I. (2011). Chemical screening in zebrafish for novel biological and therapeutic discovery. *Methods Cell Biol.* **105**, 493–516.
- Tripodo, G., Mandracchia, D., Collina, S., Rui, M., and Rossi, D. (2014). New perspectives in cancer therapy: The biotin-antitumor molecule conjugates. *Med. Chem.* **S1**, 1–8.
- Trondl, R., Heffeter, P., Kowol, C. R., Jakupec, M. A., Berger, W., and Keppler, B. K. (2014). Nkp-1339, the first ruthenium-based anticancer drug on the edge to clinical application. *Chem. Sci.* **5**, 2925–2932.
- Veinotte, C., Delleire, G., and Berman, J. (2014). Hooking the big one: The potential of zebrafish xenotransplantation to reform cancer drug screening in the genomic era. *Dis. Models Mech.* **7**, 745–754.
- Wilkinson, R. N., and van Eeden, F. J. (2014). The zebrafish as a model of vascular development and disease. *Prog. Mol. Biol. Transl. Sci.* **124**, 93–122.
- Zetter, B. R. (1998). Angiogenesis and tumor metastasis. *Annu. Rev. Med.* **49**, 407–424.
- Zhan, T., Rindtorff, N., and Boutros, M. (2017). Wnt signaling in cancer. *Oncogene* **36**, 1461–1473.
- Zhu, X. Y., Guo, D. W., Lao, Q. C., Xu, Y. Q., Meng, Z. K., Xia, B., Yang, H., Li, C. Q., and Li, P. (2019). Sensitization and synergistic anti-cancer effects of furanodiene identified in zebrafish models. *Sci. Rep.* **9**, 4541.